Downloaded from orbit.dtu.dk on: Apr 26, 2024

DTU Library

A Decade of Solid Oxide Electrolysis Improvements at DTU Energy

Hauch, Anne; Brodersen, Karen; Chen, Ming; Graves, Christopher R.; Jensen, Søren Højgaard; Jørgensen, Peter Stanley; Hendriksen, Peter Vang; Mogensen, Mogens Bjerg; Ovtar, Simona; Sun, Xiufu

Published in:
ECS Transactions

Link to article, DOI:
10.1149/07542.0003ecst

Publication date:
2017

Document Version
Peer reviewed version

Link back to DTU Orbit

Citation (APA):
Hauch, A., Brodersen, K., Chen, M., Graves, C. R., Jensen, S. H., Jørgensen, P. S., Hendriksen, P. V., Mogensen, M. B., Ovtar, S., & Sun, X. (2017). A Decade of Solid Oxide Electrolysis Improvements at DTU Energy. *ECS Transactions*, *75*(42), 3-14. https://doi.org/10.1149/07542.0003ecst

General rights
Copyright and moral rights for the publications made accessible in the public portal are retained by the authors and/or other copyright owners and it is a condition of accessing publications that users recognise and abide by the legal requirements associated with these rights.

- Users may download and print one copy of any publication from the public portal for the purpose of private study or research.
- You may not further distribute the material or use it for any profit-making activity or commercial gain
- You may freely distribute the URL identifying the publication in the public portal

If you believe that this document breaches copyright please contact us providing details, and we will remove access to the work immediately and investigate your claim.

A Decade of Solid Oxide Electrolysis Improvements at DTU Energy

A. Hauch[a], K. Brodersen[a], M. Chen[a], C. Graves[a], S. H. Jensen[a], P. S. Jørgensen[a], P. V. Hendriksen[a], M. B. Mogensen[a], S. Ovtar[a] and X. Sun[a]

[a] Department of Energy Conversion and Storage, Technical University of Denmark, Risø Campus, Frederiksborgvej 399, 4000 Roskilde, Denmark

Solid oxide electrolysis cells (SOECs) can efficiently convert electrical energy (e.g. surplus wind power) to energy stored in fuels such as hydrogen or other synthetic fuels. Performance and durability of the SOEC has increased orders of magnitudes within the last decade. This paper presents a short review of the R&D work on SOEC single cells conducted at DTU Energy from 2005 to 2015. The SOEC improvements have involved increasing the of the oxygen electrode performance, elimination of impurities in the feed streams, optimization of processing routes, and fuel electrode structure optimization. All together, these improvements have led to a decrease in long-term degradation rate from ~40 %/kh to ~0.4 %/kh for steam electrolysis at -1 A/cm^2, while the initial area specific resistance has been decreased from 0.44 Ωcm^2 to 0.15 Ωcm^2 at -0.5 A/cm^2 and 750 °C.

Introduction

Solid oxide electrolysis cells (SOECs) have the potential for efficient large-scale energy conversion from electrical energy to energy stored in fuels such as hydrogen. The energy can also be stored in more energy dense carbon-containing synthetic fuels after a catalytic upgrading from synthesis gas realized by mixing the hydrogen with CO_2 or even via internal methanation following co-electrolysis of CO_2 and steam (1–3). In this way, SOEC can become an important technology for converting CO_2 into valuable synthetic fuels. A key issue for the SOEC technology is to provide inexpensive, reliable, high performing and long-term stable SOEC for stack and system applications. Over the last decade the research activities in the field of SOEC has increased significantly. Considerable improvement has been achieved and SOEC technology is now at the verge of commercialization (4,5). This increase in SOEC research can be monitored in various ways. One way can be via the number of publications on the topic e.g. as reported by Gómez and Hotza. They reported that the number of SOEC related publications according to Scopus increased from around 20 in 2005 to approximately 110 in 2015. Meanwhile the number of solid oxide fuel cell (SOFC) related publications increased from around 900 in 2005 to 2200 in 2008 but has since then decreased to approximately 1550 in 2015 (6). DTU Energy (formerly Risø National Laboratory) has been conducting research in the field of SOEC since 2003 from performance testing of button cells to long-term reversible operation of an SOEC stack. However; this short review will only focus on the test and characterization of single cells; and provide an overview of the cell improvements and increased understanding of performance and durability as a result of SOEC research in the years from 2005 to 2015 at DTU Energy.

Figure 1 illustrates the enormous decrease in long-term degradation achieved for single cell SOEC. The long-term – almost linear – voltage degradation was decreased

from approximately 40 %/kh to 0.4 %/kh. Over the same decade, the initial performance of the single SOEC was increased significantly. As an example; for the two cells in Figure 1, the initial area specific resistance (ASR) was 0.44 Ωcm^2 for the cell tested in 2005 but only 0.15 Ωcm^2 for the cell tested in 2015, when measured at -0.5 A/cm^2 via iV-curves at 750 °C with a gas flow of $p(H_2O)/p(H_2)$:50/50 to the fuel electrode. This significant increase in initial electrochemical performance and long-term durability for the SOEC over the last decade is a result of several different steps of improvements. Figure 2 provides an illustration of the different steps on the "road-of–SOEC-improvements" from 2005 to 2015 at DTU Energy and thereby serves as an outline for this paper. Firstly, we need to treat the subject of impurities (see next section); especially considering the fact that even though solid oxide cells (SOC) are reversible cells, the effect of specific impurities are significantly different when operated as SOEC compared to SOFC. Secondly, significant and electrolysis specific degradation issues were encountered when using the composite (strontium-doped-lanthanum-manganite/yttria-stabilized-zirconia (LSM/YSZ) as oxygen electrode. This is discussed in the section "Improved Oxygen Electrodes". Improvement of both initial performance and long-term durability of the Ni/YSZ based fuel electrode is related to an altered microstructure realized by changes in the cell manufacturing process. The improved understanding of the puzzling interplay between processing, resulting microstructure and electrochemical performance achieved is described in the section "Processing and Microstructures" prior to the section on improvements for the Ni/SZ based fuel electrode.

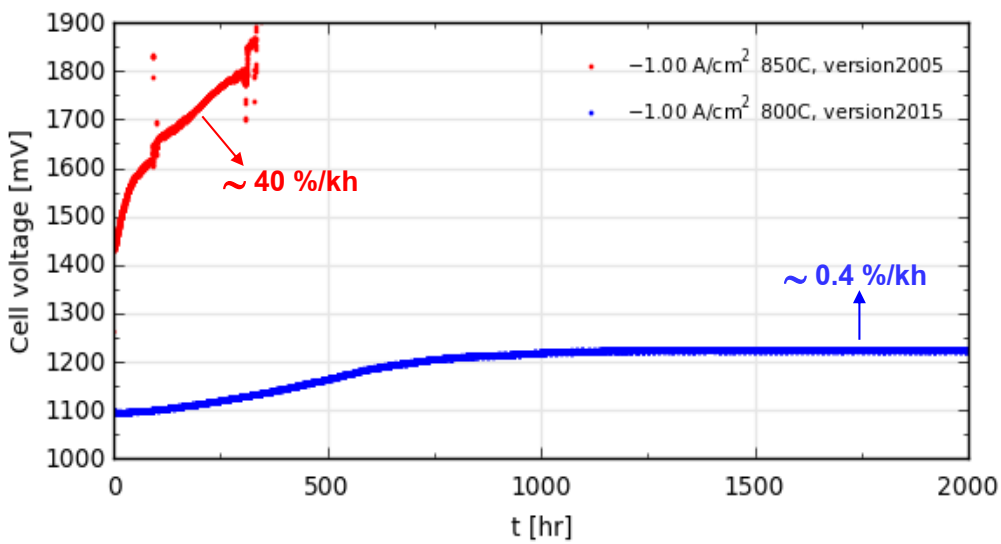

Figure 1. Cell voltage recorded over time at -1 A/cm^2 at 850 °C and 800 °C for state of the art SOEC cells prepared in 2005 and 2015 at DTU Energy (7,8). Linear voltage degradation rates are indicated.

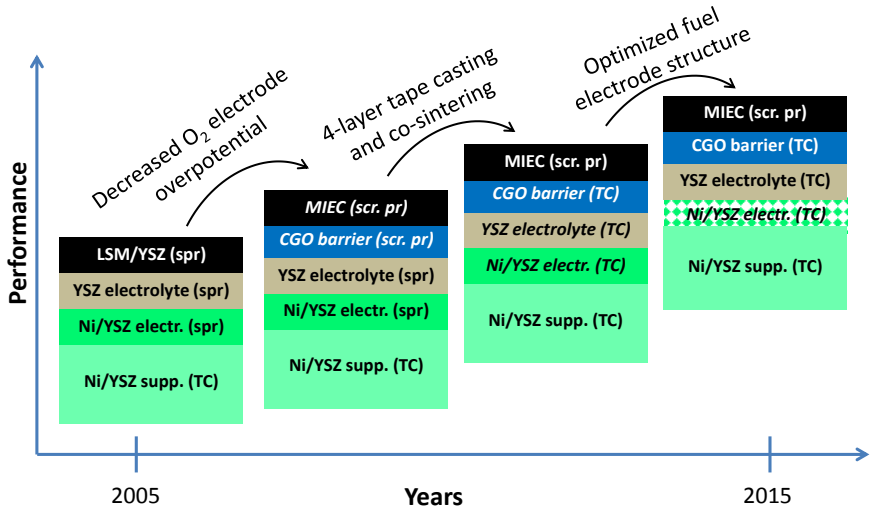

Figure 2. Sketch of SOEC single cell (planar fuel electrode supported single cells) changes from 2005 to 2015 at Risø National Lab/DTU Energy. The abbreviations are: sprayed (spr), screen printed (scr. pr) and tape cast (TC).

Effects of Impurities

There are numerous reports in literature on the effect of impurities on performance and durability of SOFC (9–18) and some research work also report on the effect of impurities on SOEC (7,19–24). In this review of SOEC improvements, we discuss two examples of impurity related SOEC degradation encountered during single cell SOEC testing at DTU Energy. That is, degradation caused by glassy phase impurities in the fuel electrodes, and sulfur sensitivity experienced under electrolysis testing in carbon containing gasses. Both examples illustrate that degradation behavior is different between SOFC and SOEC.

Glassy phase impurities

Glassy phase impurities are typically neither good conductors nor electro-catalysts for the electrochemical reactions. If these impurities are present either at the active sites for the electrochemical reaction or in-between particles, which otherwise would constitute a percolating path for either electron or ion conduction; it will inevitably lead to increased resistance of the SOEC. Figure 3 shows an EDS map of the electrolyte/fuel electrode interface for a long-term steam electrolysis tested SOEC cell (7). There are significant quantities of silica. The silica is clearly concentrated in the part of the fuel electrode closest to the electrolyte i.e. in the region of the cell where the electrochemical reactions in the fuel electrode takes place. This concentration of silica is quantified via the EDS analysis given in the left part of Figure 3; and cannot only originate from the impurities in the raw materials that are in the range of 10-15 ppm SiO_2 (25). For the case illustrated in Figure 3 the extraordinary amounts of silica-containing impurities was found to originate largely from the applied glass sealing; even though the same set-up had been applied successfully for fuel cell testing of similar cells. The differences in effect of glass sealing depending on SOFC or SOEC operation of the cells lies in the following; glass based sealing material (e.g. albite glass as applied here) will generate a certain partial pressure of $Si(OH)_4$ when exposed to a $p(H_2)/p(H_2O)$ gas stream at high temperature. The $p(Si(OH)_4)$ will increase with increasing temperature and increasing $p(H_2O)$ in the inlet gas (26). The $Si(OH)_4(g)$ is in itself not problematic and for SOFC testing the gaseous

silicon tetrahydroxide will simply pass over the cell and be part of the outlet gas stream. However, when the cell is operated in electrolysis mode, H_2O (g) is converted at the active TPB sites. This "local" consumption of H_2O (g) at and in the nano-meter vicinity of the TPB will inevitably cause the equilibrium (Le Chartelies principle) between the gaseous silicon tetrahydroxide and glassy phase silica towards the formation of silica to "release" steam for the electrolysis process; that is:

$$Si(OH)_4\ (g) \rightarrow SiO_2\ (s) + 2H_2O\ (g) \qquad (1)$$

and the glassy phase silica impurities will therefore concentrate at or in the very near vicinity of the active sites for the reduction reaction in the fuel electrode. These observations led to improved test set-up minimizing the effect of glassy phase impurities from sealing material. However, one should still pay attention to silica based impurities in SOEC even when applying test set-ups free of glass sealing for SOEC test, as evident from the reporting of trace impurities in later works (22,24,27).

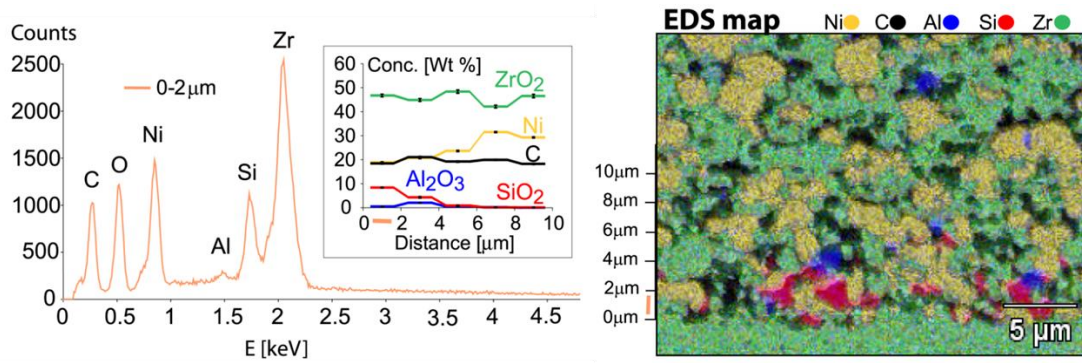

Figure 3. EDS map of Ni/YSZ electrode/electrolyte interface for a long-term tested SOEC applying a "glass-rich" sealing set-up (7).

<u>Sulfur sensitivity</u>

Only very limited results on the sensitivity of SOEC fuel electrodes towards sulfur poisoning has been reported; an "indirect" example is however given by Ebbesen et al. (19,28). Different electrolysis tests were conducted in CO_2/CO and $CO_2/H_2O/H_2$ gas mixtures leading to significant cell voltage increases even at relatively low current densities (-0.25 A/cm^2) and in-plane voltage measurements pointed towards a gas phase impurity related degradation mechanism (when compared to in-plane voltage measurements during controlled H_2S additions to the fuel inlet gas in SOFC tests). Ebbesen and co-workers reported that the supply gases could contain 5-8 ppb H_2S according to the supplier and they were able to measure, but not really quantify, H_2S in the supplied gasses. Nevertheless, cleaning of the inlet gasses lead to a significant decrease in loss of performance for the SOEC test at otherwise identical test conditions. Comprehensive test data can be found in the referenced work by Ebbesen and co-workers, while Figure 4 provides an illustrative generalized sketch of the observed cell voltage development over time for these tests.

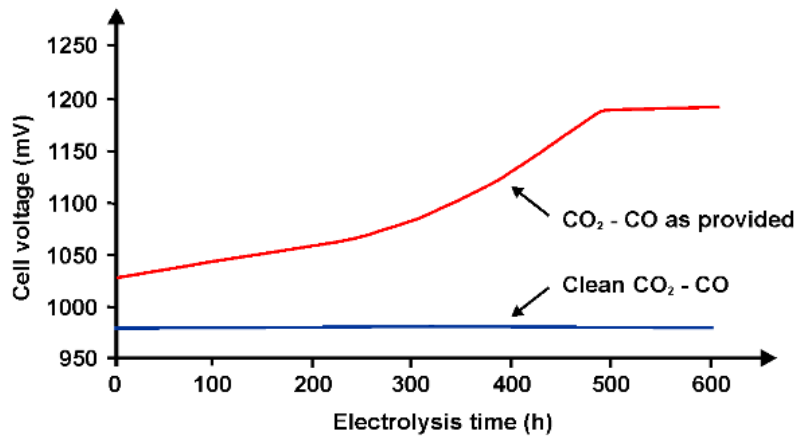

Figure 4. Sketch[1] illustrating cell voltage development during CO_2 and/or co-electrolysis at current density of -0.25 A/cm^2 and at 850 °C (19).

Later, SOEC tests by Skafte and Hauch with addition of H_2S in the range from 5 ppb to 2 ppm during co-electrolysis have confirmed the findings by Ebbesen and co-workers. The problematic impurities are especially present in the CO gas. The gases can be cleaned by simple means of crushed Ni/YSZ half-cell as a filter in the inlet gas stream as described by Ebbesen and Mogensen (29). An alternative solution for impurity removal in the gas stream (which is added only to keep the Ni in the electrode in reduced state) is re-cycling of H_2/CO, which will most likely be part of a commercial SOEC system design anyway. This means that shortly after electrolysis start-up the system will be supplied with H_2/CO from the electrolysis process and the H_2/CO will thereby be as clean as the supplied H_2O/CO_2. Also, it appears that electrolysis-induced poisoning by impurities may be mitigated by switching to fuel cell mode (25). Furthermore, periodic reversible SOEC/SOFC operation has been found to inhibit other major degradation mechanisms as well (30), such as the one described in the next section.

Improved Oxygen Electrodes

As illustrated in Figure 2 the first generation of cells tested as electrolysis cells had LSM/YSZ (lanthanum strontium doped manganite/YSZ) composite oxygen electrodes screen printed onto the dense YSZ electrolyte and sintered at ~1050 °C. This type of oxygen electrode was tested for 1500 h at 850 °C and was very stable even for fuel cell mode current densities up to 1.94 A/cm^2 (31). However, as shown by Knibbe et al. when testing similar cells for steam electrolysis at 850 °C and -2 A/cm^2 the polarization resistance increased rapidly but with a decreasing rate after a few hundred hours of testing. However, the ohmic resistance continued to increase at these test conditions. Test of a similar cell at -1 A/cm^2 did not show the same significant ohmic resistance increase. The left part of Figure 5 presents a transmission electron microscopy (TEM) image from the degraded electrolyte closest (few μm) to the oxygen electrode. The image revealed nano-scale oxygen bubbles formed in the YSZ grain boundaries. The fundamentals behind this degradation process upon operation at high current densities in electrolysis mode but not in fuel-cell mode, lies in the course of the electromotive (Fermi) potential of the electrons across the cell and how it changes from fuel cell mode across OCV to

[1] Sketch kindly provided by Dr. K. V. Hansen. Submitted by Hauch and Mogensen as contribution to "Advances in Medium and High Temperature Solid Oxide Fuel Cell Technology", Springer, 2016

electrolysis mode. The degradation mechanism is described Knibbe and co-workers (22) and detailed modeling of the potentials across the YSZ electrolyte is given by Jacobsen and co-workers (32). Upon increasing electrolysis current density the electromotive potential of the electrons in the electrolyte near the oxygen electrode increases while it decreases near the fuel electrode. At the same time the inflection point for the course of the electromotive potential in the electrolyte shifts towards the fuel electrode which further increases the oxygen potential near the electrolyte/oxygen electrode interface. The high electromotive potential near this interface causes oxygen evolution in the electrolyte YSZ grain boundaries which increases the grain boundary resistivity as observed via increasing ohmic resistance measured by electrochemical impedance spectroscopy (EIS) during electrolysis testing. This "oxygen bubble formation" degradation mechanism is outlined in the left part of Fig. 5. It will therefore be advantageous to apply oxygen electrodes with a decreased area specific resistance (ASR) to circumvent this type of irreversible degradation of the cell in order to increase the current density threshold for which this type of cell degradation is initiated.

Changing the oxygen electrode from the composite LSM/YSZ with an electron conductor (LSM) and an ion conductor (YSZ) to a mixed ionic-electronic conductor (MIEC) led to decreased oxygen electrode polarization resistance and thus lower over potential. From a more fundamental point of view it also changes the reaction mechanism from relying on a triple phase boundary (TPB) reaction site to a reaction zone for MIEC electrodes (33–35). The first MIEC based oxygen electrodes applied for SOEC at DTU Energy were based on LSCF/CGO (lanthanum-strontium-iron-cobaltite/gadolinium-doped-ceria) electrodes and the achieved long-term stability improvement was reported by Hjalmarsson et al. (36). Later, the improved LSC/CGO (lanthanum-strontium-cobaltite) has been applied. State-of-the-art LSC/CGO electrodes only contribute with a resistance of approximately 15-30 mΩcm^2 at 800 °C and typical electrolysis test conditions (- 1A/cm^2) as applied for the test depicted in Figure 1 (8).

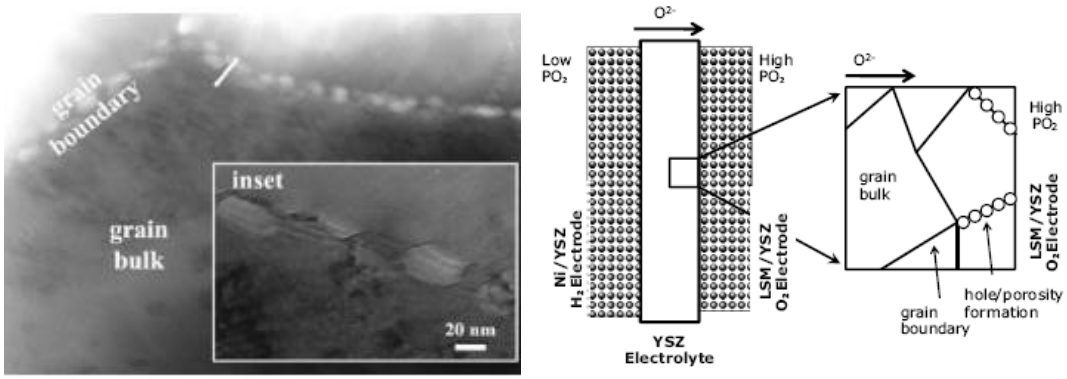

Figure 5. TEM image of oxygen bubble formations (nano-scale porosities) in the YSZ grain boundaries in the electrolyte layer closest to the LSM/YSZ oxygen electrode after H_2O electrolysis test at 850 °C and -2 A/cm^2 and sketch of the degradation mechanism. Reprint from Knibbe et al (22).

Processing and Microstructures

The processing route has changed significantly over this last decade as illustrated in Figure 2. Firstly (not shown in Figure 2), the shift from spraying to screen printing of LSM/YSZ electrodes led to improved adhesion to the sprayed YSZ electrolyte. However,

this shift did not change the electrochemical performance significantly and the electrolytes and fuel electrodes were still produced via spraying (37). The later generations of cells are based on tape casting of the fuel electrode, electrolyte and CGO barrier layer. This can be done by either multilayer tape casting or via tape casting and subsequent lamination of the layers prior to co-sintering of the entire half-cells (38–40). Several parameters (e.g. Ni/YSZ ratios, layer thicknesses, particle sizes and sintering temperature) have been investigated to optimize the production of the 4-layer co-sintered half-cells (8,40,41). In recent years processing optimization has also focused on the shift towards – if not completely water based slurries then at least - environmentally friendly production as reported by Foghmoes and co-workers (42). This will inevitably be important for large scale production of SOC.

Microstructures – and their characterization

The processing of the green body along with the sintering profile in principle lay the ground for the cell microstructures. However, one should also pay attention to the fact that the fuel electrode undergoes a reduction after the sintering step but prior to electrochemical operation. One can apply a variety of techniques to analyze electrode microstructures, but in the following we will exemplify the insight gained from two types microstructural characterization techniques: 1) 3D reconstructions applying focused ion beam slicing and SEM imaging, and 2) low-voltage in-lens SEM imaging (43).

From 3D reconstructions of electrode structures one will typically report the quantification of the TPB length, particle size distributions and phase fractions. However, even though not always reported the 3D reconstruction of the electrode microstructure also holds information on parameters such as tortuosity of the phases and the critical pathway radii. In other words how “twisted-&-turned” and how wide are the Ni “high ways” for the electrons and similarly for the O^{2-} and gasses in e.g. the fuel electrode. An illustrative example of this type of quantification of the fuel electrode structure was recently given by Jørgensen et al. who analyzed samples exposed to different reduction profiles (44). Figure 6 (left) illustrates the situation. Upon reduction of NiO the Ni network can evolve e.g. like illustrated following arrow 1 or as arrow 2. The difference between these two scenarios is interface area of the Ni particle necking as illustrated by the red line in between the Ni particles – or using the metaphor: how wide is the Ni-highway for the electrons. Figure 6 (right) shows an analysis of this necking effect through the analysis of critical pathway radii for two fuel electrodes that were cut out of the same sample but reduced at 1000 °C (HT) and at 840 °C (LT) (44), respectively. Figure 6 shows that the critical pathway radii[2] for the Ni phase is significantly different for the two electrode structures, while it is more or less identical for the zirconia and pore phases. As an example; let us imaging that a critical pathway radius of 100 nm is required to keep the percolation of the Ni network over time (arrow 3 in Figure 6) else e.g. segregated impurities or morphology changes will break up the Ni network. In this case, approximately 87 % of the initially percolating TPB sites will fulfil this requirement for the high temperature reduced cell but only around 37 % for the low temperature reduced cell.

[2] The critical pathway radius is defined as the radius of the widest pathway that can be used to reach each TPB site in the structure; i.e. the radius of the largest sphere that can pass through the network to the TPB site.

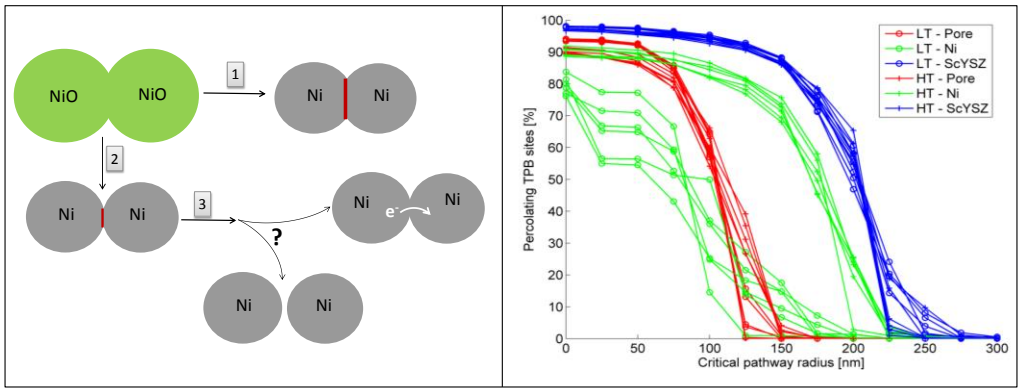

Figure 6. A schematic (left) of the Ni-network upon reduction of NiO (path 1 and 2) and upon long-term testing (path 3) and critical pathway radii (right) for two identical fuel electrodes that were reduced at 1000 °C (HT) and at 840 °C (LT) (44), respectively.

The 3D reconstructions provide very detailed microstructural insight. However, typically one will only analyze a small fraction of the electrode, e.g. volumes with side lengths of 10-20 μm. Applying low-voltage in-lens SEM imaging one will be able to investigate several millimeters of electrode in a short time and get a qualitative assessment of whether the Ni particles constituting the necessary percolating network. The next section provides an example where this method was applied in a study of loss of Ni-percolation.

Ni/YSZ Fuel Electrodes

The performance and durability of the Ni/YSZ fuel electrodes have improved significantly over this decade and the improvements rely on optimization of processing routes and resulting microstructures. Re-call the sketch in Figure 6 (arrow 3); the percolation of Ni needs to be preserved during long-term operation of the SOC. Figure 7 (top row) shows SEM images of two reference cells (pristine, i.e. only reduced) both having a Ni/YSZ ratio of 40/60 volume percent. The “old” cell (A) had a rather coarse and porous structure with a mean diameter of Ni particles in the range of 1.3 μm and a porosity of app. 36 % in the active fuel electrode. The newly produced cell (C) had finer particles, Ni mean diameter of app. 700 nm, and the active fuel electrode is made as dense as possible, which correspond to a pore fraction of 21 % for a Ni/YSZ volume ratio of 40/60 (8,39).

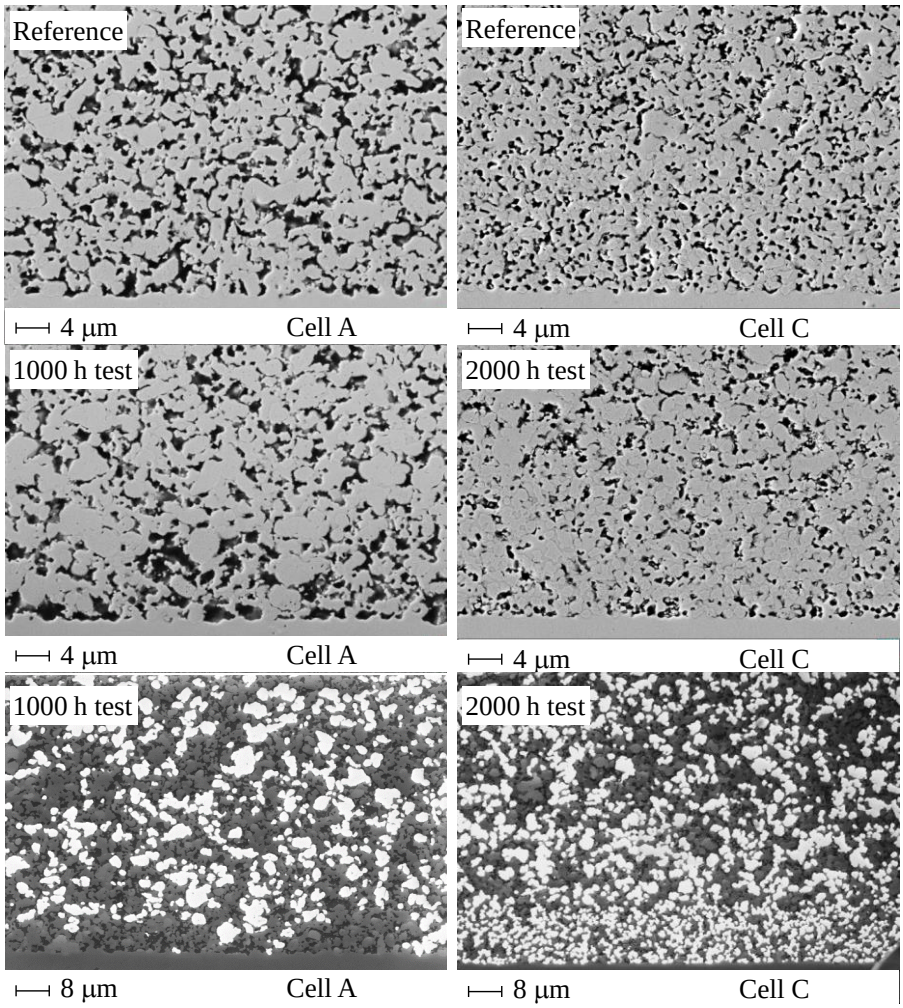

Figure 7. SEM images of cell A and cell C (optimized fuel electrode structure). Reference (as reduced) and after long-term H_2O electrolysis test as shown in Figure 8 (8).

Galvanostatic electrolysis test at 800 ºC, -1 A/cm^2, 90 % H_2O in H_2 as inlet gas and a steam conversion of 56 % was conducted for cell A and cell C. Figure 8 shows the development of cell voltage (left), R_s and R_p (right) for the two cells during electrolysis testing. Evidently cell C is the better performing. Analysis of impedance spectra recorded at these electrolysis test conditions at start of the test reveals that the polarization resistance attributed to the electrochemical reactions in the Ni/YSZ electrodes were 98 mΩcm^2 and 38 mΩcm^2 for cell A and C, respectively (8). Both cells experience an initial increase in R_p; for both cells R_p subsequently reaches a constant level. In contrast, the ohmic resistance, R_s, only increase minimally for cell C, but a substantial increase for cell A is observed. This R_s increase will inevitably be detrimental for cell A within another few thousand hours of testing. The long-term voltage degradation rate of cell C was as low as 0.4 %/kh. This corresponds to that cell C can operate just around thermoneutral potential even after 5 years of operation. Figure 7 (bottom row) illustrates the significant difference in how the electrolysis operation affected the Ni/YSZ electrodes. The Ni particles in cell C still constitute a satisfying percolating network in the entire fuel electrode and support. For cell A there is a significant lack of percolation Ni-network in the inner most 5 μm; the oxide ions thus need to be conducted through the electrolyte and further out in the YSZ network in the porous electrode to reach an active TPB. This will

lead to increased ohmic resistance (R_s). Similar examples of loss of Ni percolation and Ni migration can be found elsewhere (24,45). Both initial performance and life-time was hereby improved significantly for the Ni/YSZ electrode from cell A to cell C solely by structure optimizations.

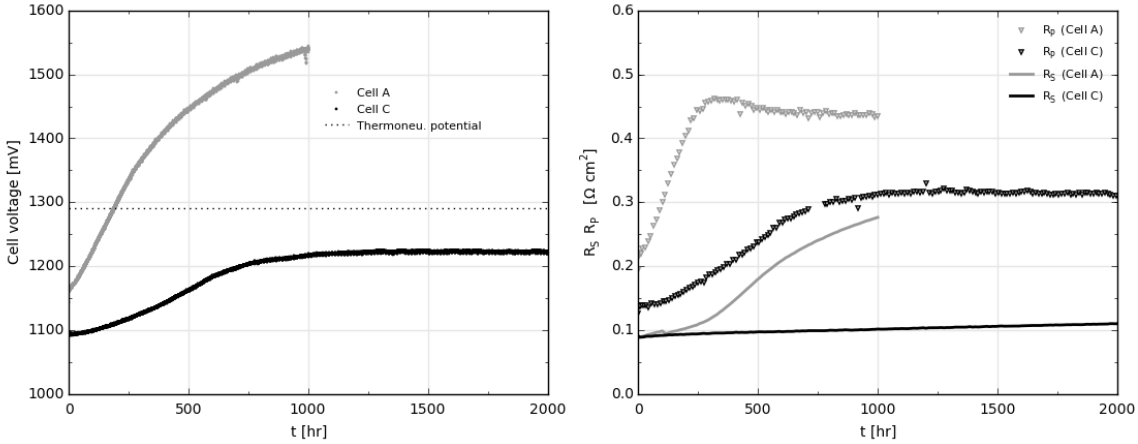

Figure 8. Development of cell voltage (left), R_s and R_p (right) for cell A and cell C during electrolysis at 800C, -1 A/cm^2, 90 % H_2O in H_2 as inlet gas and H_2O conversion of 56 % (8). R_s and R_p values are from impedance spectra recorded during electrolysis testing.

Conclusion

In conclusion, the SOEC R&D at DTU Energy from 2005 to 2015 have led to:

- A long-term degradation rate decrease from app. 40 %/kh to 0.4 %/kh (for H_2O electrolysis test of single cells at -1 A/cm^2).
- A decrease in the total initial resistance from 0.44 Ωcm^2 to 0.15 Ωcm^2 (750 °C and -0.5 A/cm^2).
- Optimized electrode structures via inexpensive up-scalable processing routes.

In parallel with the here reported improvements for single cell SOEC from 2005 to 2015 the test duration, size and complexity has changed significantly as well e.g.:

- From test run for tens or a few hundreds of hours to single cell test running for a year and SOEC stack test exceeding ½ year.
- From only galvanostatic testing, to potentiostatic testing, testing reversible operation and even SOC stack test following a wind profile and pressurized SOEC test (2,30,46).
- Last but not least improvements in characterization of SOEC e.g. from impedance spectroscopy only at OCV for single cells to impedance spectroscopy for individual large cells in a stack under current load (47).

Acknowledgments

The authors would like to thank colleges at DTU Energy, especially Mr. H. Henriksen and Ms M. Davodi for technical assistance and Dr. K. V. Hansen for Figure 4. Furthermore, the authors acknowledge the financial support from the ForskEL project “Towards Solid Oxide Electrolysis Plants in 2020”

References

1. X. Sun, M. Chen, S. H. Jensen, S. D. Ebbesen, C. Graves and M. B. Mogenen, *Int. J. Hydrogen Energy*, **37**, 17101–17110 (2012).
2. S. H. Jensen, X. Sun, S. D. Ebbesen, R. Knibbe, and M. Mogensen, *Int. J. Hydrogen Energy*, **35**, 9544–9549 (2010).
3. C. Graves, S. D. Ebbesen, M. Mogensen, and K. S. Lackner, *Renew. Sustain. Energy Rev.*, **15**, 1–23 (2011). http://linkinghub.elsevier.com/retrieve/pii/S1364032110001942.
4. SunFire Gmbh, press release Feb 29th 2016; *http://www.sunfire.de/en/company/press/detail/sunfire-supplies-boeing-with-worlds-largest-commercial-reversible-electrolysis-rsoc-system-16*
5. GasInnovations, press release Feb. 3rd 2016; *http://www.prnewswire.com/news-releases/gas-innovations-changes-landscape-of-carbon-monoxide-market-300214036.htm*.
6. S. Y. Gómez and D. Hotza, *Renew. Sustain. Energy Rev.*, **61**, 155–174 (2016).
7. A. Hauch, S. H. Jensen, J. B. Bilde-Sørensen, and M. Mogensen, *J. Electrochem. Soc.*, **154**, A619 (2007).
8. A. Hauch, K. Brodersen, M. Chen, and M. B. Mogensen, *Solid State Ionics*, **293**, 27–36 (2016).
9. M. S. Schmidt, K. V Hansen, K. Norrman, and M. B. Mogensen, *Solid State Ionics*, **179**, 1436–1441 (2008).
10. K. Vels Hansen and M. B. Mogensen, *Electrochem. Solid-State Lett.*, **15**, B70 (2012).
11. K. V Jensen, R. Wallenberg, I. Chorkendorff, and M. Mogensen, *Solid State Ionics*, **160**, 27–37 (2003).
12. Y. L. Liu, S. Primdahl, and M. Mogensen, *Solid State Ionics*, **161**, 1–10 (2003).
13. J. F. B. Rasmussen and A. Hagen, *Fuel Cells*, **10**, 1135–1142 (2010).
14. A. Hagen, *J. Electrochem. Soc.*, **160**, F111–F118 (2013).
15. A. Hauch, A. Hagen, J. Hjelm, and T. Ramos, *J. Electrochem. Soc.*, **161**, F734–F743 (2014).
16. H. Madi, A. Lanzini, S. Diethelm, D. Papurello, J. Van Herle, and M. Lualdi, *J. Power Sources*, **279**, 460–471 (2015).
17. K. Haga, S. Adachi, Y. Shiratori, K. Itoh, and K. Sasaki, *Solid State Ionics*, **179**, 1427–1431 (2008).
18. D. Papurello, A. Lanzini, S. Fiorilli, F. Smeacetto, R. Singh, M. Santarelli, *Chem. Eng. J.*, **283** (2016).
19. S. D. Ebbesen, C. Graves, A. Hauch, S. H. Jensen, and M. Mogensen, *J. Electrochem. Soc.*, **157**, B1419 (2010).
20. D. Wiedenmann, A. Hauch, B. Grobéty, M. B. Mogensen, and U. F. Vogt, *Int. J. Hydrogen Energy*, **35**, 5053–5060 (2010).
21. A. Hauch, J. R. Bowen, L. T. Kuhn, and M. B. Mogensen, *Electrochem. Solid-State Lett.*, **11**, B38 (2008).
22. R. Knibbe, M. L. Traulsen, A. Hauch, S. D. Ebbesen, and M. B. Mogensen, *J. Electrochem. Soc.*, **157**, B1209 (2010).
23. R. Kiebach, K. Norrman, C. Chatzichristodoulou, M. Chen, X. Sun, S. D. Ebbesen, M. B. Mogensen, P. V. Hendriksen, *Dalton Trans.*, **43**, 14949–58 (2014).
24. M. Chen, Y-L. Liu, J J Bentzen, W. Zhang, X. Sun, A. Hauch, Y. Tao, J. R.

Bowen, P. V. Hendriksen, *J. Electrochem. Soc.*, **160**, F883–F891 (2013)
25. A. Hauch, S. H. Jensen, S. Ramousse and M. B. Mogensen, *J. Electrochem. Soc.*, **153**, A1741 (2006).
26. R. Knibbe, A. Hauch, J. Hjelm, S. D. Ebbesen, and M. Mogensen, *Green*, **1**, 141–169 (2011).
27. A. Hauch, PhD Thesis, Technical University of Denmark (2007).
28. S. D. Ebbesen and M. Mogensen, *J. Power Sources*, **193**, 349–358 (2009).
29. S. Ebbesen and M. B. Mogensen, Patent, WO2013026555 (2013).
30. C. Graves, S. D. Ebbesen, S. H. Jensen, S. B. Simonsen, and M. B. Mogensen, *Nat. Mater.*, **14**, 239–44 (2015).
31. A. Hagen, R. Barfod, P. V Hendriksen, Y. L. Liu, and S. Ramousse, *J. Electrochem. Soc.*, **153**, A1165–A1171 (2006).
32. T. Jacobsen, C. Chatzichristodoulou, and M. B. Mogensen, *ECS Trans.*, **61**, 203–214 (2014).
33. M. Backhaus-Ricoult, *Solid State Sci.*, **10**, 670–688 (2008).
34. J. Hjelm, M. Søgaard, R. Knibbe, A. Hagen, and M. B. Mogensen, *ECS Transactions*, **13**, 285–299 (2008).
35. J. Nielsen and J. Hjelm, *Electrochim. Acta*, **115**, 31–45 (2014).
36. P. Hjalmarsson, X. Sun, Y.-L. Liu, and M. Chen, *J. Power Sources*, **223**, 349–357 (2013).
37. S. Ramousse, M. Menon, K. Brodersen, J. Knudsen, U. Rahbek and P. H. Larsen, *ECS Trans.*, **7**, 317–327 (2007).
38. P. H. Larsen and K. Brodersen, patent, US2008124602-A1; JP2008130568-A; EP1930974-A1; CN101242003-A; CA2611362-A1; KR2008047282-A; KR966845-B1 (2008).
39. K. Brodersen, A. Hauch, M. Chen, and J. Hjelm, Patent Application No 1518138.3 (2015).
40. A. Hauch, C. Birkl, K. Brodersen, and P. S. Jørgensen, *Proc. 10th European Solid Oxide Fuel Cell Forum*, **Chapter 8**, 62–71 (2012).
41. A. Hauch, F. Karas, K. Brodersen, and M. Chen, in *Proc. 11th European SOFC and SOE Forum*, p. 88 (2014).
42. S. Foghmoes, F. Teocoli, K. Brodersen, T. Klemensø, and M. Della Negra, *J. Eur. Ceram. Soc.*, **36**, 3441 (2016).
43. K. Thydén, Y.-L. Liu, and J. B. Bilde-Sørensen, *Solid State Ionics*, **178**, 1984–1989 (2008).
44. P. S. Jørgensen, S. L. Ebbehøj, and A. Hauch, *J. Power Sources*, **279**, 686–693 (2015).
45. Y. Tao, S. D. Ebbesen, and M. B. Mogensen, *J. Power Sources*, **328**, 452–462 (2016).
46. X. Sun, A. D. Bonaccorso, C. Graves, S. D. Ebbesen, S. H. Jensen, A. Hagen, P. Holtappels, P. V. Hendriksen, and M. B. Mogensenet, *Fuel Cells*, **15**, 697–702 (2015).
47. R. R. Mosbæk, J. Hjelm, R. Barfod, J. Høgh, and P. V. Hendriksen, *Fuel Cells*, **13**, 605–611 (2013).